The Plant Cell, Vol. 32: 1905–1918, June 2020, www.plantcell.org © 2020 ASPB.

Control of Grain Size and Weight by the GSK2-LARGE1/OML4 Pathway in Rice

Jia Lyu,[a,1] Dekai Wang,[b,1] Penggen Duan,[a,1] Yapei Liu,[a,1] Ke Huang,[a,c] Dali Zeng,[d] Limin Zhang,[a] Guojun Dong,[d] Yingjie Li,[a,c] Ran Xu,[a] Baolan Zhang,[a] Xiahe Huang,[e] Na Li,[a] Yingchun Wang,[e] Qian Qian,[d,2] and Yunhai Li[a,c,2]

[a] State Key Laboratory of Plant Cell and Chromosome Engineering, CAS Centre for Excellence in Molecular Plant Biology, Institute of Genetics and Developmental Biology, The Innovative Academy of Seed Design, Chinese Academy of Sciences, Beijing, 100101, China

[b] College of Life Sciences and Medicine, Zhejiang Sci-Tech University, Hangzhou, 310018, China

[c] University of Chinese Academy of Sciences, Beijing, 100039, China

[d] State Key Laboratory of Rice Biology, China National Rice Research Institute, Hangzhou 310006, China

[e] State Key Laboratory of Molecular Developmental Biology, Institute of Genetics and Developmental Biology, Chinese Academy of Sciences, Beijing, 100101, China

ORCID IDs: 0000-0001-7927-1791 (J.L.); 0000-0002-0557-6864 (D.W.); 0000-0002-3301-819X (P.D.); 0000-0001-7592-8549 (Y.P.L.); 0000-0003-4832-9692 (K.H.); 0000-0003-2349-8633 (D.Z.); 0000-0003-1536-0378 (L.Z.); 0000-0002-7556-4404 (G.D.); 0000-0002-3774-6055 (Y.J.L.); 0000-0002-8253-0288 (R.X.); 0000-0003-0856-345X (B.Z.); 0000-0001-6495-2594 (X.H.); 0000-0003-3975-7951 (N.L.); 0000-0002-9150-3556 (Y.W.); 0000-0002-0349-4937 (Q.Q.); 0000-0002-0025-4444 (Y.H.L.)

Regulation of grain size is crucial for improving crop yield and is also a basic aspect in developmental biology. However, the genetic and molecular mechanisms underlying grain size control in crops remain largely unknown despite their central importance. Here, we report that the MEI2-LIKE PROTEIN4 (OML4) encoded by the *LARGE1* gene is phosphorylated by GLYCOGEN SYNTHASE KINASE2 (GSK2) and negatively controls grain size and weight in rice (*Oryza sativa*). Loss of function of *OML4* leads to large and heavy grains, while overexpression of *OML4* causes small and light grains. OML4 regulates grain size by restricting cell expansion in the spikelet hull. *OML4* is expressed in developing panicles and grains, and the GFP-OML4 fusion protein is localized in the nuclei. Biochemical analyses show that the GSK2 physically interacts with OML4 and phosphorylates it, thereby possibly influencing the stability of OML4. Genetic analyses support that GSK2 and OML4 act, at least in part, in a common pathway to control grain size in rice. These results reveal the genetic and molecular mechanism of a GSK2-OML4 regulatory module in grain size control, suggesting that this pathway is a suitable target for improving seed size and weight in crops.

INTRODUCTION

The world population continues to increase rapidly, and this increase has led to a growing demand for rice (*Oryza sativa*; Lee et al., 2015). Grain yield is determined by tiller number, grain number, and grain weight. As grain size is a key component of grain weight, regulation of grain size is a crucial strategy to increase grain production. Grain growth is restricted by spikelet hulls, which influence final grain size in rice (Li and Li, 2016; Li et al. 2019). The growth of the spikelet hull is determined by cell proliferation and cell expansion processes. Several genes that regulate the grain size by influencing cell proliferation in the spikelet hull have been described in rice, such as *GRAIN WIDTH AND WEIGHT2* (*GW2*; Song et al., 2007), *GRAIN SIZE ON CHROMOSOME5* (*GW5/GSE5*; Duan et al., 2017; Liu et al., 2017), *GRAIN WIDTH ON CHROMOSOME8* (*GW8/OsSPL16*; Wang et al., 2012), *GRAIN SIZE ON CHROMOSOME3* (*GS3*; Fan et al., 2006; Li et al., 2011), *GRAIN SHAPE ON CHROMOSOME9* (*GS9*; Zhao et al., 2018), *OsMKKK10-OsMKK4-OsMPK6* (Duan et al., 2014; Xu et al. 2018a, 2018b), and Mitogen-activated protein Kinase Phosphatase1 (*MKP1*; Guo et al., 2018; Xu et al., 2018b). In addition, several genes that control grain size by influencing cell expansion in the spikelet hulls have been reported in rice, such as *GRAIN SIZE ON CHROMOSOME2* (*GS2/OsGRF4*; Che et al., 2015; Duan et al., 2015; Hu et al., 2015), *GSK3/SHAGGY-like kinase5* (*OsGSK5*; Hu et al., 2018; Xia et al., 2018; Ying et al., 2018), *GRAIN LENGTH AND WEIGHT ON CHROMOSOME7* (*GLW7/SPL13*; Si et al., 2016), *GRAIN LENGTH ON CHROMOSOME7* (*GL7/GW7/SLG7*; Wang et al., 2015a, 2015b; Zhou, 2015), *POSITIVE REGULATOR OF GRAIN LENGTH1/2* (*PGL1/PGL2*; Heang and Sassa, 2012a, 2012b), and *ANTAGONIST OF PGL1* (*APG*; Heang and Sassa, 2012a, 2012b). However, the genetic and molecular relationships between these factors remain largely unknown.

SHAGGY-LIKE KINASE2 (GSK2), a homologue of the Arabidopsis (*Arabidopsis thaliana*) BRASSINOSTEROID INSENSITIVE2 (BIN2) kinase, has been reported to influence grain size and also other growth processes in rice (Tong et al., 2012). Overexpression of *GSK2* leads to small grains and short plants, whereas downregulation of *GSK2* produces long grains. GSK2

[1] These authors contributed equally to this work.

[2] Address correspondence to yhli@genetics.ac.cn or qianqian188@hotmail.com.

The author responsible for distribution of materials integral to the findings presented in this article in accordance with the policy described in the Instructions for Authors (www.plantcell.org) is: Yunhai Li (yhli@genetics.ac.cn).

www.plantcell.org/cgi/doi/10.1105/tpc.19.00468

can associate with and phosphorylate DWARF AND LOW-TILLERING (DLT). Interestingly, downregulation of *DLT*/*GS6* causes multiple growth defects as well as wide, short, and heavy grains due to increased cell proliferation in the grain-width direction (Sun et al., 2013). GSK2 also interacts with the transcription factor OsGRF4/GS2 described to influence grain growth predominantly by promoting cell expansion in the spikelet hull (Che et al., 2015; Duan et al., 2015; Hu et al., 2015). A recent study has shown that GW5/GSE5, a calmodulin binding protein, can associate with GSK2 and repress its kinase activity (Duan et al., 2017; Liu et al., 2017). GW5/GSE5 regulates grain width by limiting cell proliferation in the spikelet hull (Duan et al., 2017; Liu et al., 2017). However, genetic interactions between GSK2 and these grain size regulators are not clear so far.

To further reveal the mechanisms of grain size determination, we have identified several grain size genes whose loss and gain of function lead to opposite effects on grain size in rice. Here, we report that *LARGE1*, which encodes MEI2-LIKE PROTEIN4 (OML4) with three RNA recognition motif (RRM) domains, regulates grain size and weight by restricting cell expansion in spikelet hulls in rice. Homologs of OML4 have been reported to influence meiosis, the plastochron, and leaf maturation in plant species (Veit et al., 1998; Kaur et al., 2006; Kawakatsu et al., 2006; Xiong et al., 2006), but their function in seed/grain size control has not been characterized so far. The *large1-1* mutant forms large and heavy grains, while overexpression of *OML4* causes small and light grains. OML4 interacts with GSK2 and can be phosphorylated by GSK2. Genetic analyses indicate that GSK2 and OML4 function, at least in part, in a common pathway to control grain size. Therefore, our findings reveal a significant genetic and molecular mechanism of the GSK2-OML4 regulatory module in grain size control, suggesting that it is useful for grain size and weight improvement in crops.

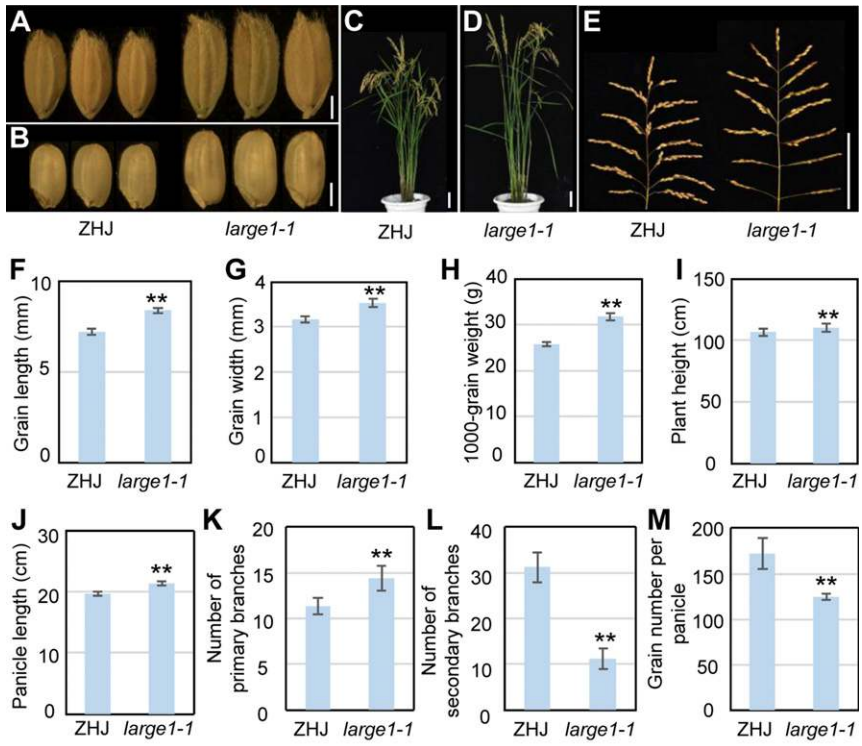

Figure 1. *LARGE1* Influences Grain Size and Plant Morphology.

(A) Mature paddy grains of ZHJ and *large1-1*.
(B) Brown rice grains of ZHJ and *large1-1*.
(C) and **(D)** ZHJ **(C)** and *large1-1* **(D)** plants at mature stage.
(E) ZHJ (left) and *large1-1* (right) panicles.
(F) and **(G)** Grain length **(F)** and width **(G)** of ZHJ and *large1-1*.
(H) The 1000-grain weight of ZHJ and *large1-1*.
(I) Plant height of ZHJ and *large1-1*.
(J) Panicle length of ZHJ and *large1-1*.
(K) Number of ZHJ and *large1-1* primary panicle branches.
(L) Number of ZHJ and *large1-1* secondary panicle branches.
(M) Grain number per panicle of ZHJ and *large1-1*.
Values (**[F]** to **[H]**) are given as mean ± SD ($n \geq 50$). Values (**[I]** to **[M]**) are given as means ± SD ($n = 20$). Asterisks indicate significant differences between ZHJ and *large1-1*. **, $P < 0.01$ compared with the wild type (ZHJ) by Student's *t* test. Bar in **(A)** and **(B)** = 2 mm; bar in **(C)** to **(E)** = 10 cm.

RESULTS

The *large1* Mutant Forms Large and Heavy Grains

We have previously identified a number of grain size mutants in rice. The *large1-1* mutant was isolated from γ-ray–treated M2 populations of the *japonica* var Zhonghuajing (ZHJ). The *large1-1* mutant displayed large grains and tall plants (Figures 1A to 1E). The length of *large1-1* grains was increased by 16.24% compared with that of ZHJ grains (Figure 1F). Similarly, the width of *large1-1* grains was increased by 11.54% compared with that of ZHJ grains (Figure 1G). The *large1-1* grains were also significantly heavier than ZHJ grains (Figure 1H). The weight of *large1-1* grains was increased by 23.11% compared with that of ZHJ grains. These results indicate that *LARGE1* negatively regulates grain size and weight in rice.

Mature *large1-1* plants were significantly higher than ZHJ plants (Figure 1I). The *large1-1* panicles were long and loose in comparison with the wild-type panicles (Figure 1J), indicating that *LARGE1* also negatively influences panicle length. As panicle structure and shape are determined by panicle branches, we investigated ZHJ and *large1-1* panicle branches. The primary branches of *large1-1* panicles were more than those of ZHJ (Figure 1K), and the *large1-1* had fewer secondary branches than ZHJ (Figure 1L). We also investigated the number of grains per panicle in ZHJ and *large1-1*. The number of grains per panicle in *large1-1* was decreased in comparison with that in ZHJ (Figure 1M). These results suggest that *LARGE1* influences the balance between grain number and grain size in rice.

LARGE1 Regulates Cell Expansion in Spikelet Hulls

Grain growth is limited by spikelet hulls, and spikelet hull growth is determined by cell proliferation and cell expansion processes (Li and Li, 2016). To uncover the cellular mechanism for *LARGE1* in grain growth, we investigated cells in ZHJ and *large1-1* spikelet hulls. As shown in Figure 2, the outer epidermal cells in *large1-1* lemmas were longer and wider cells than those of ZHJ lemmas, while cell numbers in *large1-1* lemmas were similar to that in the wild-type lemmas in both longitudinal and transverse directions (Figures 2A, 2B, and 2E to 2H). Similarly, the inner epidermal cells of *large1-1* were longer and wider than those of ZHJ (Figures 2C, 2D, 2I, and 2J). These results indicate that the long and wide grain phenotypes of *large1-1* result from the long and wide cells in spikelet hulls. Thus, *LARGE1* regulates grain size by limiting cell expansion in spikelet hulls.

As several genes were reported to regulate grain size by influencing cell expansion in spikelet hulls, we investigated their expression levels in the wild-type and *large1-1* panicles (Supplemental Figure 1). SPL13/GWL7, a transcription factor, positively influences grain length by increasing cell expansion (Si et al., 2016). Higher expression of *SPL13* in *large1-1* panicles was observed. *GL7* promotes cell elongation in spikelet hulls, resulting in long grains (Wang et al., 2015a, 2015b; Zhou et al., 2015), although *GL7/GW7/SLG7* is also proposed to increase grain length by influencing cell proliferation (Wang et al., 2015b). Expression of *GL7* was obviously increased in *large1-1* compared with ZHJ (Supplemental Figure 1). The putative Ser carboxypeptidase GS5

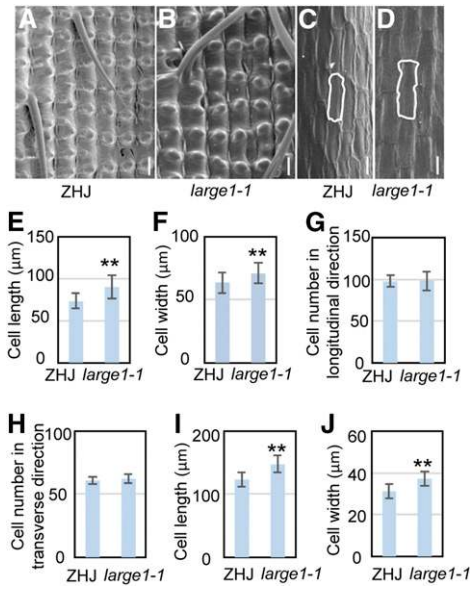

Figure 2. *large1* Forms Large Grains Due to Increased Cell Expansion in the Spikelet Hull.

(A) and **(B)** Scanning electron microscopy analysis of the outer surface of ZHJ **(A)** and *large1-1* **(B)** lemmas.
(C) and **(D)** Scanning electron microscopy analysis of the inner surface of ZHJ **(C)** and *large1-1* **(D)** lemmas.
(E) and **(F)** Average length **(E)** and width **(F)** of outer epidermal cells in ZHJ and *large1-1* lemmas.
(G) Outer epidermal cell number in the longitudinal direction in ZHJ and *large1-1* lemmas.
(H) Outer epidermal cell number in the transverse direction in ZHJ and *large1-1* lemmas.
(I) and **(J)** Average length **(I)** and width **(J)** of inner epidermal cells in the longitudinal direction in ZHJ and *large1-1* lemmas.
Values (**[E]** to **[J]**) are given as the means ± SD ($n \geq 50$). **, $P < 0.01$ compared with the wild type by Student's *t* test.
Bar in **(A)** to **(D)** = 50 μm.

and the transcription factor GS2 affect grain growth by increasing both cell expansion and cell proliferation (Li et al., 2011; Duan et al., 2015; Hu et al., 2015). Expression levels of *GS5* and *GS2* in *large1-1* were significantly higher than those in ZHJ (Supplemental Figure 1). The basic helix-loop-helix transcription factor PGL1 controls grain length by increasing cell expansion (Heang and Sassa, 2012a, 2012b). APG, another basic helix-loop-helix transcription factor, regulates grain length by restricting cell expansion in spikelet hulls (Heang and Sassa, 2012a, 2012b). Expression of *APG* and *PGL1* in *large1-1* was lower and higher than that in ZHJ, respectively (Supplemental Figure 1). These data indicate that *LARGE1* influences the expression of several grain size genes that regulate cell expansion.

LARGE1 Encodes the Mei2-Like Protein OML4

The MutMap approach was used to identify the *large1-1* mutation (Abe et al., 2012; Fang et al., 2016; Huang et al., 2017). We crossed ZHJ with *large1-1* and generated an F2 population. In the F2 population, the progeny segregation showed that the single

recessive mutation determines the large-grain phenotype of *large1-1*. The genomic DNAs from F2 plants with the large-grain phenotype were pooled and applied for whole-genome re-sequencing. The wild-type ZHJ was also sequenced as a control. Single-nucleotide polymorphism (SNP) analyses were performed as described previously (Fang et al., 2016; Huang et al., 2017). We detected 3913 SNPs and 1280 small insertions and deletions (INDELs) between ZHJ and the pooled F2 plants with *large1-1* phenotypes. The SNP:INDEL ratio in the pooled F2 plants was calculated in the whole genome (Supplemental Figure 2). Among them, only one INDEL in the coding region had an SNP:INDEL ratio = 1. This INDEL contained a 4-bp deletion in *large1-1* in the gene (*LOC_Os02g31290*; Figure 3A; Supplemental Figure 3; Supplemental Table 1), which leads to a premature stop codon (Figure 3B). We further confirmed this deletion in *LOC_Os02g31290* by developing a derived cleaved-amplified polymorphic sequence marker (Figure 3C). These results indicate that *LOC_Os02g31290* is the candidate gene for *LARGE1*.

A genetic complementation test was conducted to confirm whether the deletion in *LOC_Os02g31290* was responsible for the *large1-1* phenotypes. The genomic fragment of *LOC_Os02g31290* (*gLARGE1*) was transformed into the *large1-1* mutant, and 11 transgenic lines were generated. The *gLARGE1* construct complemented the large-grain phenotypes of the

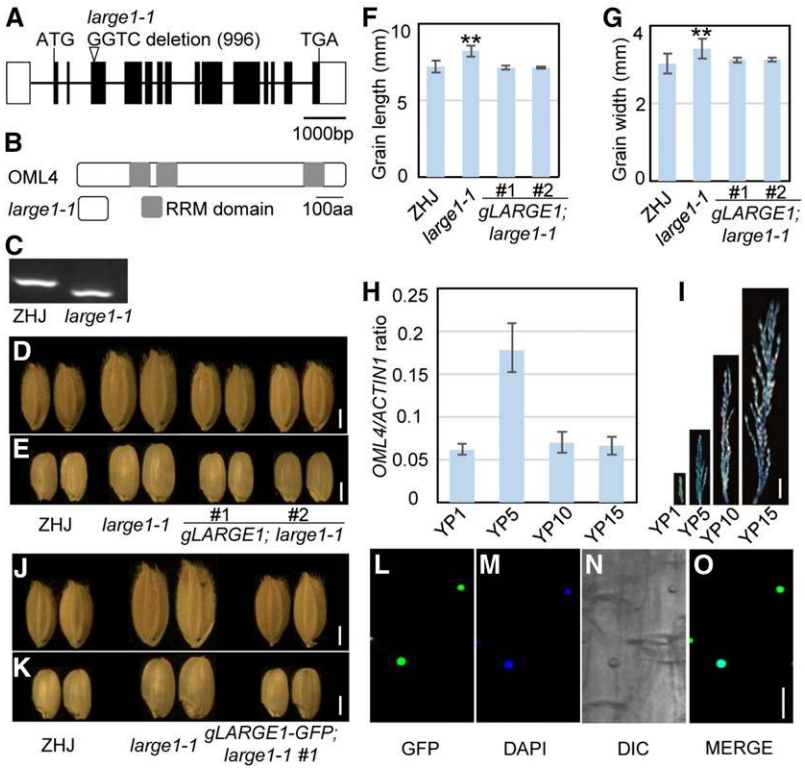

Figure 3. *LARGE1* Encodes the Mei2-Like Protein OML4.

(A) *LARGE1/OML4* gene structure. The coding sequence is shown as the black box, and introns are indicated using black lines. ATG and TGA represent the start codon and the stop codon, respectively.

(B) OML4 and mutated protein encoded by *large1*. The OML4 protein contains three RRM domains. The mutation results in a premature termination codon in *OML4*, causing a truncated protein.

(C) Derived cleaved-amplified polymorphic sequence marker was developed according to the *large1-1* mutation. The PCR products were digested by the restriction enzyme *Hph*I.

(D) and **(E)** Mature paddy **(D)** and brown **(E)** rice grains of ZHJ, *large1-1*, *gLARGE1;large1-1 #1*, and *gLARGE1;large1-1 #2*.

(F) and **(G)** Grain length **(F)** and width **(G)** of ZHJ, *large1-1*, *gLARGE1;large1-1 #1*, and *gLARGE1;large1-1 #2*. Asterisks indicate significant differences between ZHJ and *large1-1*. **, $P < 0.01$ compared with the wild type by Student's *t* test.

(H) Relative *OML4* gene expression in young panicles of 1 cm (YP1) to 15 cm (YP15) in ZHJ. RT-qPCR was used to measure expression levels of *OML4* in panicles. Values are given as mean ± SD. Three biological replicates were used ($n = 3$).

(I) *OML4* expression activity was monitored by *proOML4*:*GUS* transgene expression. Histochemical analysis of GUS activity in panicles at different developmental stages.

(J) and **(K)** Mature paddy **(J)** and brown **(K)** rice grains of ZHJ, *large1-1*, and *gLARGE1-GFP;large1-1 #1*.

(L) to **(O)** Subcellular location of OML4-GFP in *gLARGE1-GFP;large1-1 #1* root cells. GFP fluorescence of GFP-OML4 **(L)**, 4′,6-diamidino-2-phenylindole staining (DAPI; see **[M]**), differential interference contrast (DIC; see **[N]**), and merged **(O)** images are shown.

Bar in **(D)**, **(E)**, **(J)**, and **(K)** = 2 mm; bar in **(I)** = 1 cm; bar in **(L)** to **(O)** = 10 μm.

large1-1 mutant (Figures 3D and 3E). The grain length and width of *gLARGE1;large1-1* transgenic plants were similar to those of ZHJ (Figures 3F and 3G). Genomic complementation plants also recovered to the wild type in plant height and morphology (Supplemental Figure 4). Therefore, the complementation test supported that the *LARGE1* gene is *LOC_Os02g31290*.

LARGE1/LOC_Os02g31290 encodes the OML4 with three RRMs (Figure 3B; Supplemental Figure 5). Homologs of OML4 were found in crops and mammals (Supplemental Figures 5 and 6; Supplemental Data Set). Homologs of OML4 were reported to influence meiosis, the plastochron, and leaf maturation in plants (Veit et al., 1998; Kaur et al., 2006; Kawakatsu et al., 2006; Xiong et al., 2006), but the roles of OML4 and its homologs in grain size control are totally unknown so far. The mutation in *large1-1* resulted in a premature stop codon. The proteins encoded by *large1-1* ($OML4^{large1\text{-}1}$) lacked RRM motifs (Figure 3B), which indicated that *large1-1* is a loss-of-function allele.

Expression and Subcellular Localization of OML4

We investigated the expression of *OML4* in developing panicles using RT-qPCR analysis. The *OML4* gene expression was detected and was also variable during panicle development (Figure 3H). We further generated the *OML4* promoter:GUS transgenic plants (*proOML4*:*GUS*) and examined the expression patterns of *OML4* in developing panicles. During panicle development, β-glucuronidase (GUS) activity was detected in the panicles with ~1 cm of length. The strongest GUS activity was observed in the panicles with ~5 cm of length. The GUS activity then gradually decreased during panicle development (Figure 3I). Similarly, RT-qPCR analysis indicate that expression of *OML4* was relatively high in the panicles with ~5 cm of length (Figure 3H).

To investigate the subcellular localization of OML4 in rice, we generated *gLARGE1-GFP* transgenic plants. As shown in Figures 3J and 3K, the *gLARGE1-GFP* construct rescued the phenotypes of the *large1-1* mutant, indicating that the LARGE1-GFP fusion protein is functional. GFP signal in *gLARGE1-GFP;large1-1* roots was predominantly detected in nuclei (Figures 3L to 3O). Thus, this finding indicated that OML4 is localized in nuclei in rice.

Overexpression of *OML4* Results in Short Grains Due to Short Cells in Spikelet Hulls

To further explore the functions of *OML4* in grain growth, we generated the *proActin*:*OML4* construct, transformed it into ZHJ, and isolated 14 transgenic lines. The *proActin*:*OML4* transgenic plants had short grains compared with ZHJ (Figures 4A to 4C), while the width of *proActin*:*OML4* grains was similar to that of ZHJ (Figure 4D). The grains were also significantly lighter than those of ZHJ (Figure 4E). Grain length of *proActin*:*OML4* transgenic lines was associated with the expression levels of *OML4* (Figure 4F). These data reveal that *OML4* functions to restrict grain growth in rice.

Mature *proActin*:*OML4* transgenic plants were shorter than ZHJ (Figures 4G and 4H). The average length of *proActin*:*OML4* panicles was significantly decreased compared with that of ZHJ panicles (Figures 4I and 4J). The primary panicle branches of *proActin*:*OML4* were comparable to those of ZHJ, while the secondary panicle branches of *proActin*:*OML4* were obviously increased in comparison to those of ZHJ (Figures 4K and 4L), resulting in the increased grain number per panicle (Figure 4M).

As *proActin*:*OML4* transgenic lines produced short grains, we tested whether overexpression of *OML4* could decrease cell length in spikelet hulls. We examined the size of outer epidermal cells in the wild-type and *proActin*:*OML4* spikelet hulls (Figures 4N and 4O). Outer epidermal cells in *proActin*:*OML4* spikelet hulls were shorter than those of ZHJ spikelet hulls (Figures 4P and 4Q). By contrast, the number of epidermal cells in the longitudinal and transverse direction in *proActin*:*OML4* spikelet hulls was similar to that in ZHJ spikelet hulls (Figures 4R and 4S). These results further revealed that *OML4* affects grain growth by limiting cell expansion in spikelet hulls.

OML4 Interacts with GSK2

To further understand the molecular role of OML4 in grain growth control, we identified its interacting partners through a yeast two-hybrid assay (Supplemental Table 2). The OML4 full-length protein was used as the bait. Among several interacting proteins, six different clones corresponding to GSK2 were found in this screen. GSK2 has been reported to restrict grain growth in rice (Tong et al., 2012), suggesting that GSK2 is a candidate OML4-interacting partner. We further confirmed the interaction of OML4 with the full-length GSK2 in yeast cells (Figure 5A).

We next verified the interaction between OML4 and GSK2 in plant cells using the firefly luciferase (LUC) complementation imaging assay (Figure 5B). The OML4-nLUC and GSK2-cLUC constructs (nLUC, N-terminal luciferase; cLUC, C-terminal luciferase) were transformed and coexpressed in *Nicotiana benthamiana* leaves. The LUC activity was detected when we coexpressed OML4-nLUC and GSK2-cLUC, while no signal was observed in both combinations of OML4-nLUC/cLUC and nLUC/GSK2-cLUC. We then performed a bimolecular fluorescence complementation (BiFC) assay to test the interaction between OML4 and GSK2 in plant cells (Figure 5C). OML4 was fused with the C terminus of the yellow fluorescent protein (OML4-cYFP), and GSK2 was fused with the N terminus of the yellow fluorescent protein (GSK2-nYFP). Confocal laser-scanning microscopy observation showed strong YFP fluorescence in nuclei when we coexpressed OML4-cYFP and GSK2-nYFP in *N. benthamiana* leaves. These results indicate that OML4 associates with GSK2 in plant cells.

To investigate whether OML4 could directly interact with GSK2, we performed an in vitro pull-down assay (Figure 5D). We expressed maltose binding protein (MBP)–fused OML4 (OML4-MBP) and glutathione S-transferase (GST) tag–fused GSK2 (GSK2-GST) proteins in *Escherichia coli* cells. As shown in Figure 5D, OML4-MBP physically interacted with GSK2-GST, but not the negative control (GST) in vitro. The coimmunoprecipitation analyses were used to examine the association of GSK2 and OML4 in *N. benthamiana*. We coexpressed GSK2-GFP and OML4-MYC in *N. benthamiana* leaves (Figure 5E). Total proteins were isolated and incubated with MYC beads to immunoprecipitate OML4-MYC. The anti-MYC and anti-GFP antibodies were

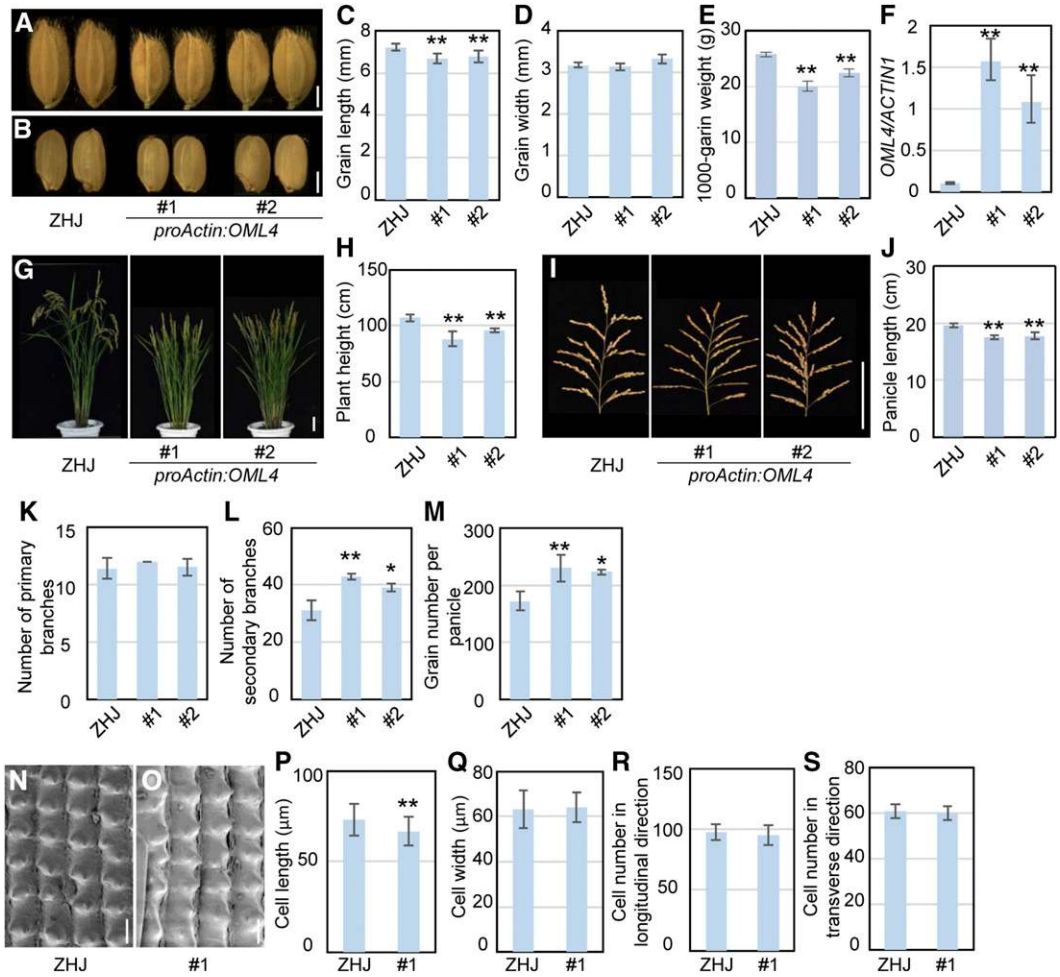

Figure 4. Overexpression of *OML4* Results in Smaller Grains.

(A) and **(B)** Mature paddy **(A)** and brown rice **(B)** grains of ZHJ and *proActin*:*OML4*.
(C) and **(D)** Grain length **(C)** and width **(D)** of ZHJ and *proActin*:*OML4* transgenic lines.
(E) The 1000-grain weight of ZHJ and *proActin*:*OML4* transgenic lines.
(F) Expression level of *OML4*/*LARGE1* in ZHJ and *proActin*:*OML4* transgenic lines. RT-qPCR was used to measure expression levels of *OML4*/*LARGE1*. Three biological replicates were used ($n = 3$). *ACTIN1* was used to normalize expression.
(G) ZHJ and *proActin*:*OML4* plants.
(H) Plant height of ZHJ and *proActin*:*OML4* transgenic lines.
(I) ZHJ and *proActin*:*OML4* panicles.
(J) Panicle length of ZHJ and *proActin*:*OML4* transgenic lines.
(K) and **(L)** Primary **(K)** and secondary **(L)** panicle branch number of ZHJ and *proActin*:*OML4* transgenic lines.
(M) Total grain number per panicle of ZHJ and *proActin*:*OML4* transgenic lines.
(N) and **(O)** Scanning electron microscopy analysis of the outer surface of ZHJ **(N)** and *proActin*:*OML4 #1* **(O)** lemmas.
(P) and **(Q)** Average length **(P)** and width **(Q)** of outer epidermal cells in the longitudinal direction in ZHJ and *proActin*:*OML4 #1* lemmas.
(R) and **(S)** Number of outer epidermal cells in the longitudinal **(R)** and transverse **(S)** direction in ZHJ and *proActin*:*OML4 #1* lemmas.
Values (see **[C]** to **[E]** and **[P]** to **[S]**) are given as the means ± SD ($n \geq 50$). Values (see **[F]**) are given as the mean ± SD. Values (see **[H]** and **[J]** to **[M]** are given as the means ± SD ($n = 20$). Asterisks indicate significant differences between ZHJ and *proActin*:*OML4* transgenic lines. *, $P < 0.05$; **, $P < 0.01$ compared with the wild type by Student's *t* test.
Bar in **(A)** and **(B)** = 2 mm; bar in **(G)** and **(I)** = 10 cm; bar in **(N)** and **(O)** = 50 μm.

used to detect immunoprecipitated proteins. GSK2-GFP proteins were detected in the immunoprecipitated OML4-MYC complexes (Figure 5E), indicating that GSK2 associated with OML4 in vivo. These results reveal that OML4 can directly interact with GSK2 in vitro and in vivo.

GSK2 Phosphorylates OML4 and Modulates Its Protein Level

As GSK2 possesses kinase activity and interacts with OML4, we examined whether GSK2 could phosphorylate OML4. To test this,

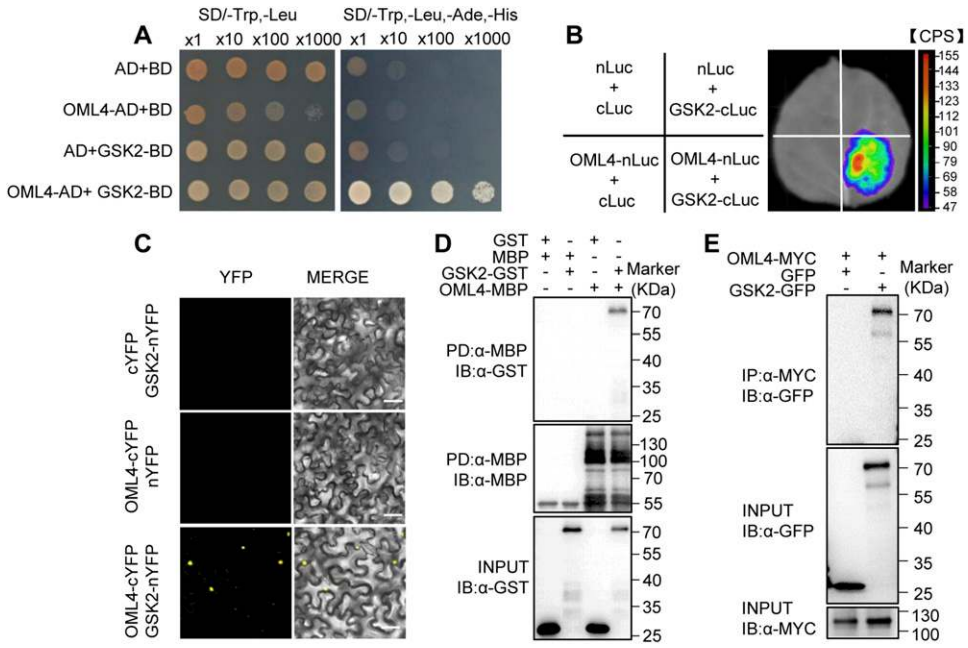

Figure 5. OML4 Physically Interacts with GSK2 in Vitro and in Vivo.

(A) OML4 interacts with GSK2 in yeast cells. Yeast cells were cultured on SD/-Trp-Leu or SD/-Trp-Leu-His-Ade media. AD, GAL4 activation domain; BD, GAL4 DNA-binding domain; SD, synthetic defined.

(B) OML4 associates with GSK2 in *N. benthamiana*. OML4-nLUC and GSK2-cLUC were coexpressed in *N. benthamiana* leaves. LUC activity was observed 48 h after infiltration. The range of luminescence intensity is indicated by the pseudocolor scale bar.

(C) BiFC assays showing that OML4 interacts with GSK2 in *N. benthamiana*. OML4-cYFP was coexpressed with GSK2-nYFP in leaves of *N. benthamiana.* Bar = 50 μm.

(D) OML4 binds GSK2 in vitro. GSK2-GST was incubated with OML4-MBP and pulled down by OML4-MBP and detected by immunoblot with anti-GST antibody. IB, immunoblot.

(E) Interaction between OML4 and GSK2 in the coimmunoprecipitation assays. Anti-MYC beads were used to immunoprecipitate GSK2-GFP proteins. Gel blots were probed with anti-MYC or anti-GFP antibody. IB, immunoblot.

we performed an in vitro kinase assay. GST-fused GSK2 (GSK2-GST) proteins were incubated with OML4-Flag, the N-terminal region of OML4-fused Flag (nOML4-Flag), and the C-terminal region of OML4-fused Flag (cOML4-Flag) in an in vitro kinase assay buffer. Phosphorylated OML4-Flag, nOML4-Flag, and cOML4-Flag were detected in the presence of GSK2-GST, while the phosphorylated OML4-Flag, nOML4-Flag, and cOML4-Flag proteins were not found in the absence of GSK2-GST (Figure 6A). These results show that GSK2 can phosphorylate OML4 in vitro.

To further verify that GSK2 can phosphorylate OML4, we investigated phosphorylation sites of OML4. To identify the phosphorylation sites in OML4, the recombinant OML4 was incubated with the recombinant GSK2 in an in vitro kinase assay buffer, separated by SDS-PAGE electrophoresis, and then subjected to liquid chromatography–tandem mass spectrometry (LC-MS/MS) analysis for phosphopeptides. We identified 18 phosphopeptides of OML4, which corresponded to 14 phosphosites (Figure 6B; Supplemental Figure 7; Supplemental Table 3). Among 14 phosphorylation sites of OML4, we observed that Ser-105, Ser-146, and Ser-607 are Ser/Thr, Ser, and Ser in its closest homologs in different plant species, respectively (Supplemental Figure 8), suggesting that these three amino acids are possible conserved phosphorylation sites. We then mutated two amino acids into phosphor-dead Ala (OML4^{S105A,S607A}) and detected their phosphorylation levels by GSK2. Mutations of the two aforementioned Ser residues to Ala reduced the phosphorylation level of OML4, although OML4^{S105A,S607A} was still phosphorylated by GSK2 (Figures 6C and 6D), indicating that Ser-105 and Ser-607 partially contribute to its phosphorylation by GSK2. This result further supports that GSK2 can phosphorylate OML4 in vitro.

Considering that GSK2 can interact with and phosphorylate OML4 in vitro, we asked whether the protein level of OML4 could be affected by GSK2. As shown in Figure 6E, we found that the level of OML4-MYC was increased when GSK2-GFP was coexpressed in leaves of *N. benthamiana*. Considering that the phosphorylation level of OML4^{S105A,S607A} was lower than that of OML4 in vitro, we asked whether mutations in Ser-105 and Ser-607 could influence the protein level of OML4. As shown in Figure 6F, the level of OML4^{S105A,S607A} was obviously lower than that of OML4 when we transiently overexpressed GSK2-GFP with OML4-MYC or OML4^{S105A,S607A}-MYC in leaves of *N. benthamiana.* These results indicate that GSK2 affects the level of OML4, possibly by influencing its phosphorylation.

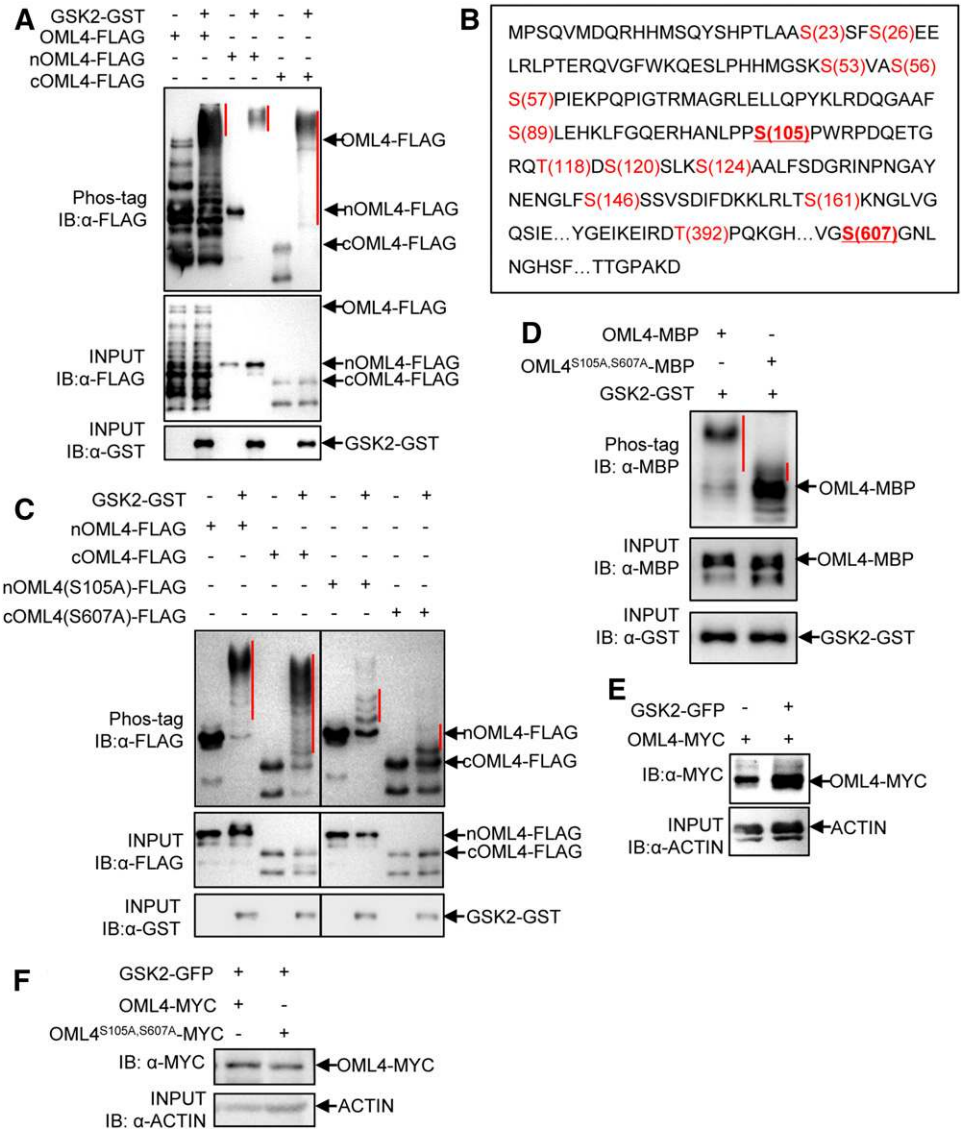

Figure 6. GSK2 Is Required for the Phosphorylation of OML4.

(A) GSK2 phosphorylates OML4 in vitro. The phosphorylated OML4-FLAG, nOML4-FLAG (the N terminus of OML4) and cOML4-FLAG (the C terminus of OML4) were separated by phos-tag SDS-PAGE. The phosphorylated protein is marked with the red vertical line. IB, immunoblot.
(B) Detection of phosphorylation sites of OML4 by LC-MS/MS after in vitro phosphorylation. OML4 contains 1001 residues. The phosphorylate residues detected by LC-MS/MS are shown in red. Two important residues (underlined) were substituted with phosphor-dead residues.
(C) Ser-105 and Ser-607 partially influence the phosphorylation of OML4. The phosphorylated nOML4-FLAG, nOML4(S105A)-FLAG, cOML4-FLAG, and cOML4(S607A)-FLAG were separated by phos-tag SDS-PAGE. The phosphorylated protein is marked with the red vertical line.
(D) Ser-105 and Ser-607 partially influence the phosphorylation of OML4. The phosphorylated OML4-MBP, OML4^{S105A,S607A}-MBP and GSK2-GST were separated by phos-tag SDS-PAGE. The phosphorylated protein is marked with red vertical line. IB, immunoblot.
(E) *GSK2* influences the abundance of OML4. GSK2-GFP and OML4-MYC were coexpressed in *N. benthamiana* leaves, and protein levels were detected by immunoblotting (IB). This experiment was repeated three times, with similar results.
(F) Ser-105 and Ser-607 partially influence the abundance of OML4. GSK2-GFP and OML4-MYC or OML4^{S105A,S607A}-MYC were coexpressed in *N. benthamiana* leaves and protein levels were detected by immunoblotting (IB). This experiment was repeated three times, with similar results.

GSK2 Acts Genetically with *OML4* to Regulate Grain Size

Although GSK2 has been described to affect grain size, the function of GSK2 in grain size control has not been characterized in detail. To investigate in detail the role of GSK2 in grain size control, we downregulated the expression of *GSK2* using RNA interference (RNAi; *GSK2-RNAi*), as described previously (Tong et al., 2012). *GSK2-RNAi* lines showed longer and slightly wider

grains than ZHJ (Figures 7A to 7E), indicating that GSK2 predominantly regulates grain length in rice. The grain weight of *GSK2-RNAi* transgenic lines was also significantly increased in comparison with that of ZHJ (Figure 7F). We then observed epidermal cells in ZHJ and *GSK2-RNAi* spikelet hulls. *GSK2-RNAi* spikelet hulls contained longer and slightly wider epidermal cells than ZHJ spikelet hulls (Figures 7G to 7J). By contrast, cell number in the grain-length and grain-width directions in *GSK2-RNAi* lemmas was similar to that in the wild-type lemmas (Figures 7K and 7L). These results demonstrate that *GSK2* controls grain growth by limiting cell elongation in spikelet hulls.

GSK2-RNAi produced long grains, like those observed in the *large1-1* mutant, and GSK2 and OML4 restrict cell elongation in spikelet hulls (Figures 2 and 7). In addition, GSK2 can phosphorylate OML4 in vitro. We therefore speculated that GSK2 and OML4 could function in a common pathway to regulate grain length in rice. To test this hypothesis, we crossed *large1-1* with *GSK2-RNAi* and isolated *large1-1;GSK2-RNAi* plants (Figure 7M). As shown in Figure 7N, the length of *large1-1* grains was increased by 16.24% in comparison with that of ZHJ, while the length of *large1-1;GSK2-RNAi* grains was increased by 7.90% compared with *GSK2-RNAi*. The results suggest that GSK2 acts, at least in

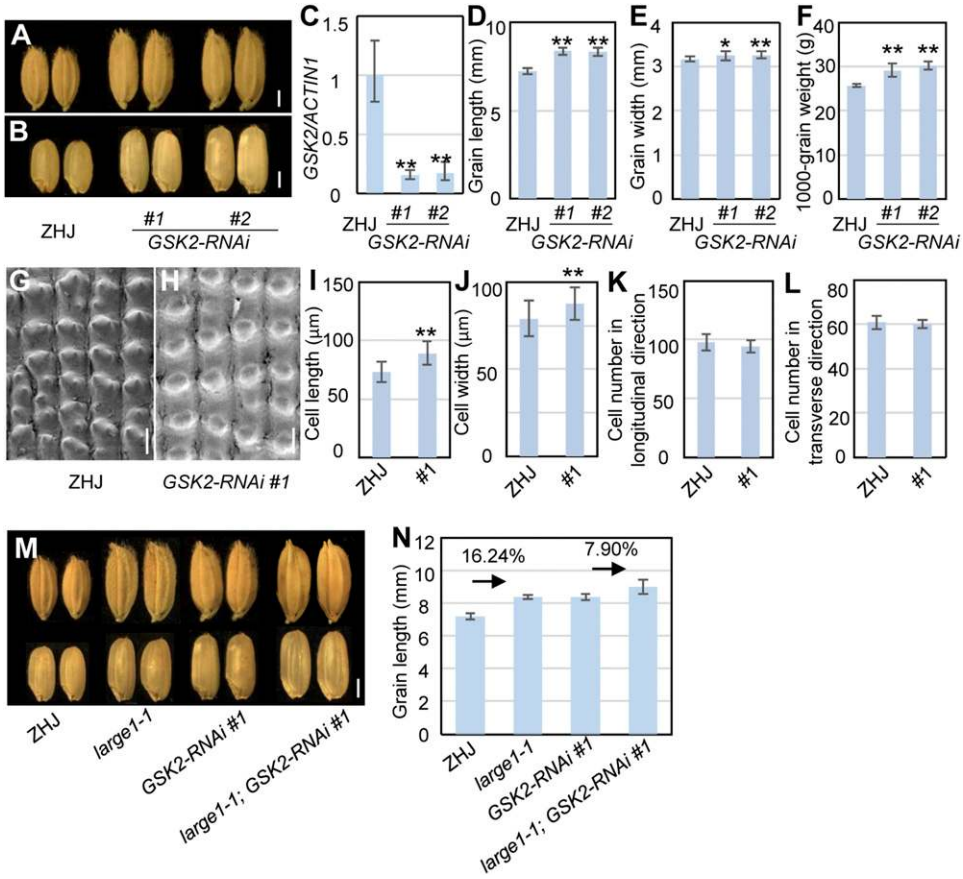

Figure 7. *GSK2* Acts Genetically with *OML4* to Regulate Seed Size.

(A) Mature paddy grains of ZHJ and *GSK2-RNAi*.

(B) Brown rice grains of ZHJ and *GSK2-RNAi*.

(C) Expression level of *GSK2* in ZHJ and *GSK2-RNAi* transgenic lines. RT-qPCR was used to measure expression levels of *GSK2*. Three biological replicates were used ($n = 3$). *ACTIN1* was used to normalize expression.

(D) and **(E)** Grain length **(D)** and width **(E)** of ZHJ and *GSK2-RNAi* transgenic lines.

(F) The 1000-grain weight of ZHJ and *GSK2-RNAi* transgenic lines.

(G) and **(H)** Scanning electron microscopy analysis of the outer surface of ZHJ **(G)** and *GSK2-RNAi #1* **(H)** lemmas.

(I) and **(J)** Average length **(I)** and width **(J)** of outer epidermal cells in the longitudinal direction in ZHJ and *GSK2-RNAi #1* lemmas.

(K) and **(L)** Number of outer epidermal cells in the longitudinal **(K)** and transverse **(L)** direction in ZHJ and *GSK2-RNAi #1* lemmas.

(M) Grains of ZHJ, large1-1, GSK2-RNAi#1, and large1-1; GSK2-RNAi#1.

(N) Grain length of ZHJ, large1-1, GSK2-RNAi#1 and large1-1; GSK2-RNAi#1.

Values (**[D]** to **[F]**, **[I]** to **[L]**, and **[N]**) are given as the means ± SD ($n \geq 50$). *, $P < 0.05$; **, $P < 0.01$ compared with the wild type by Student's *t* test.

Bar in **(A)**, **(B)**, and **(M)** = 2 mm; bar in **(G)** and **(H)** = 50 μm.

part, in a common genetic pathway with OML4 to control grain length.

As GSK2 acts as a negative regulator of brassinosteroid (BR) signaling, and GSK2-RNAi lines are sensitive to BR (Tong et al., 2012), we tested whether the *large1-1* mutant could be involved in BR responses. Previous studies revealed that the roots of the wild-type plants become curly after BR treatment. We therefore examined the BR response of the *large1-1* mutant by treatment with different concentrations of epi-brassinolide (epi-BL). In half-strength Murashige and Skoog medium without epi-BL, the roots of *large1-1* were similar to those of ZHJ (Supplemental Figure 9A). However, in half-strength Murashige and Skoog medium with epi-BL, the roots of *large1-1* seedlings were more curved than those of ZHJ (Supplemental Figure 9B). We also performed a lamina joint bending assay for BR sensitivity. The *large1-1* mutant showed more bending than ZHJ in response to BR treatment (Supplemental Figures 9C to 9E). These findings indicated that *large1-1* is more sensitive to epi-BL. Expression levels of BR-related genes, including *DWARF*, *D2*, *BZR1*, and *D61*, in *large1-1* were significantly higher than those in ZHJ (Supplemental Figure 9F). Thus, it is plausible that the GSK2-OML4 module is involved in BR responses.

Nucleotide Diversity and Selection Signatures

Previous studies showed that the chromosome region covering *OML4* contains multiple quantitative-trait loci for grain size and weight (Gao et al., 2004; Marri et al., 2005; Wan et al., 2005), suggesting that this region could be selected by breeders. To test this, we investigated the nucleotide diversity of a 10,200-bp genomic fragment containing the *OML4* gene in wild and cultivated rice using 446 *Oryza rufipogon* and 1083 *O. sativa* varieties (Huang et al., 2012). We measured the ratio of the genetic diversity in wild rice to that in cultivated rice (π_W:π_C). The nucleotide diversity of this region was reduced in cultivated rice in comparison with wild rice (Supplemental Figure 10A). The ratio of the genetic diversity $\pi_{O.\,rufipogon}$:$\pi_{O.\,sativa}$ was 3.145 (Supplemental Figure 10B), which was higher than the genome-wide threshold of selection signals (π_W:$\pi_C > 3$; Huang et al., 2012). These results suggest that this region could have selective signatures in the full population.

The population structures of the 446 *O. rufipogon* accessions were classified into three types, simply designated as Or-I, Or-II, and Or-III (Huang et al., 2012). A previous study showed that *O. s. indica* and *japonica* are descended from Or-I and Or-III, respectively (Huang et al., 2012). We then investigated the nucleotide diversity between *japonica* and Or-III and that between *indica* and Or-I. The ratio of the genetic diversity $\pi_{Or\text{-}III}$:$\pi_{japonica}$ was 13.046 (Supplemental Figure 10B), which was lower than the genome-wide threshold of selection signals (π_W:$\pi_C < 14$; Huang et al., 2012). The ratio of the genetic diversity $\pi_{Or\text{-}I}$:π_{indica} was 2.610 in this whole region and 4.127 in the 5′-flanking region, respectively (Supplemental Figure 10B), while the genome-wide threshold of selection signals was below 3 (π_W:$\pi_C < 3$). These results suggest that a part of this region could have selective signatures in the *indica* population, but not in the *japonica* population.

DISCUSSION

Grain size and weight are critical determinants of grain yield, but the genetic and molecular mechanisms of grain size control in rice are still unlcear. In this study, we identify OML4 as a regulator of grain size and weight. GSK2 interacts with and phosphorylates OML4. GSK2 and OML4 function, at least in part, in a common pathway to control grain length in rice. These findings reveal an important genetic and molecular mechanism of the GSK2-OML4 regulatory module in grain size control.

The *large1-1* mutant produced long, wide, and heavy grains in comparison to the wild type. By contrast, overexpression of *LARGE1* caused short and light grains. Thus, *LARGE1* is a negative regulator of grain size and weight. Cellular analyses support that *LARGE1* controls grain size by restricting cell expansion. Consistent with this, expression of several genes (e.g., *SPL13*, *GS2*, *GS5*, and *GL7*; Li et al., 2011; Che et al., 2015; Duan et al., 2015; Hu et al., 2015; Zhou et al., 2015; Si et al., 2016), which control grain size by regulating cell expansion, was altered in *large1-1*. The *large1-1* plants also formed long panicles with increased primary panicle branches and decreased secondary panicle branches, resulting in a reduction in grain number per panicle (Figure 1M). This result suggests that LARGE1 influences the balance between grain size and grain number per panicle. Consistent with this idea, several genes have been shown to affect the trade-off between grain size and grain number per panicle. For example, mutations in *MKP1* resulted in an increase in grain size and a decrease in grain number per panicle (Guo et al., 2018; Xu et al., 2018). Similarly, overexpression of constitutively active *OsMKKK10* produced long panicles with large grains and reduced grain number per panicle (Xu et al., 2018). It is an important challenge to understand how LARGE1 regulates the trade-off between grain size and grain number per panicle in the future. In addition, the LARGE1 influences plant height. These results indicate that LARGE1 regulates both vegetative and reproductive organ growth in rice.

LARGE1 encodes a Mei2-like protein (OML4) in rice. There are many Mei2-like proteins in plants that have the conserved RRMs but appear to have taken on distinct functions in plant development (Jeffares et al., 2004). The *Arabidopsis-Mei2-Like* (*AML*) genes comprise a five-member gene family that plays a role in meiosis and vegetative growth (Kaur et al., 2006). In maize (*Zea mays*), *terminal ear1* (*te1*), encoding a Mei2-like protein, plays a role in regulating leaf initiation (Veit et al., 1998). In rice, *PLASTOCHRON2* (*PLA2*)/*LEAFY HEAD2* (*LHD2*) encodes a Mei2-like protein (OML1; Kawakatsu et al., 2006). The *pla2* mutant exhibited precocious maturation of leaves, a shortened plastochron, and ectopic shoot formation during the reproductive phase (Kawakatsu et al., 2006). However, a function for Mei2-like proteins in seed/grain size control has not been reported in plants. In this study, we identify OML4 as a negative regulator of grain size in rice.

The LARGE1/OML4 protein contains three RRM domains. RRMs are found in a variety of RNA binding proteins. For example, Arabidopsis FCA, which contains two RRMs, controls flowering time by binding the cold-induced antisense transcript *COOLAIR* (Tian et al., 2019). In rice, PigmR-INTERACTING and BLAST RESISTANCE PROTEIN1 (PIBP1), an RRM protein, functions as

a transcription factor to regulate the defense genes expression (Zhai et al., 2019). In our study, expression of several grain size genes and BR-related genes was altered in the *large1-1* mutant. It will be worthwhile to test whether LARGE1/OML4 could bind mRNAs, miRNAs, or noncoding RNAs and associate with the promoters to regulate their expression in the future.

We further identified OML4-interacting proteins. Interestingly, one of them is the GSK2, a homologue of Arabidopsis BIN2 kinase, which has been reported to influence grain size and multiple growth processes in rice (Tong et al., 2012). Previous studies showed that GSK2 interacts with several grain size regulators. However, the effect of GSK2 on cell proliferation and/or cell expansion in spikelet hulls has not been characterized in detail. In this study, we found that downregulation of *GSK2* formed large grains as a result of large cells in spikelet hulls. These results indicate that *GSK2* restricts cell expansion rather than cell proliferation in spikelet hulls. Consistent with this, it has been proposed that GSK2 regulates grain size by interacting with GS2 that predominately promotes cell expansion in spikelet hulls (Che et al., 2015). GSK5, a homolog of GSK2, has been reported to control grain size by restricting cell expansion in spikelet hulls (Hu et al., 2018). Considering that GSK2 is a functional protein kinase, we presumed that GSK2 could phosphorylate OML4. Consistent with this idea, we found that GSK2 can interact with and phosphorylate OML4. We further observed that GSK2 influences the level of OML4. It is possible that GSK2 might phosphorylate OML4 and prevent the degradation of OML4. Supporting this, we observed that mutations in Ser-105 and Ser-607 partially influence the abundance of OML4. Our genetic analyses suggest that GSK2 and OML4 function, at least in part, in a common pathway to control grain length in rice. In addition, we found that *large1-1* is hypersensitive to epi-BL, like *GSK2-RNAi* plants. The *large1-1* mutation also influences the expression of several BR-related genes. It is possible that the GSK2-OML4 module may provide a link between BRs and grain growth. Therefore, our findings reveal an important genetic and molecular mechanism of grain size control involving the GSK2-OML4 regulatory module in rice, suggesting this module is a promising target for grain size improvement in crops.

METHODS

Plant Materials and Growth Conditions

γ-Rays were used to irradiate the grains of the wild-type ZHJ, and the *large1-1* mutant was isolated from the M2 population. Rice (*Oryza sativa*) plants were grown in the field according to a previous report (Huang et al., 2017). Rice plants were cultivated at Lingshui from December 2016 to April 2017 and from December 2017 to April 2018 and at Zhejiang (Hangzhou) from July 2017 to November 2017 and from July 2018 to November 2018.

Phenotypic Evaluation and Cellular Analysis

The ZHJ and *large1-1* plants grown in the paddy fields were taken photographs after completing ripe. A Scan Marker i560 (MICROTEK) was used to scan mature seeds. We use the Rice Test System (WSeen) to measure the grain length and width. We also measured the 1000-grain weight with three replicates (separate samples from the same experiment; Huang et al., 2017). We used a scanning electron microscope to observe the cell size and cell number. Observation via scanning electron microscopy was performed as previously described by Duan et al. (2015). ImageJ software was used to measure cell length and width.

RNA Extraction and RT-qPCR Analysis

Total RNA of seedlings of ZHJ, *proActin*:*OML4* transgenic lines, and *GSK2-RNAi* transgenic lines or young panicles of 1, 5, 10, and 15 cm from ZHJ were extracted using an RNA Pre Pure Plant Kit (Tiangen). cDNAs were synthesized according to a previous study (Duan et al., 2015). qPCR was conducted on an ABI7500 real-time PCR system using a SYBR Green Mix Kit (Bio-Rad). Rice *ACTIN1* was used as an internal control. Primers for RT-qPCR are shown in Supplemental Table 4.

Identification of the *LARGE1* Gene

We crossed *large1-1* with the wild-type ZHJ to produce F2 populations. We cloned the *LARGE1* gene using the F2 population. The whole genomes of the wild-type ZHJ and a mixed pool of 50 individual plants with mutant phenotypes were resequenced using a NextSeq 500 system (Illumina). MutMap was used to isolate *LARGE1* as previously described by Abe et al. (2012), and the SNP:INDEL ratio was analyzed as previously described by Fang et al. (2016).

Constructs and Plant Transformation

The genomic sequence of *OML4*, which contained a 2049-bp 5′-flanking region, the whole gene region, and a 1259-bp 3′-flanking region, was amplified using the primers gOML4-99-F and gOML4-99-R. We used the GBclonart Seamless Cloning Kit to fuse the *OML4* genomic sequence to the *pMDC99* vector and generated the *gOML4* recombinant construct. The latter series of the recombinant vectors was constructed using the same kit and similar methods. The related vectors we used in this study were *pIPKB003* (containing the *ACTIN* promoter and fused with the coding sequence of the *OML4* gene), *pMDC107* (constructing the *gOML4-GFP* plasmid), and *pMDC164* (constructing the *proOML4*:*GUS* vector). Primers used for constructs are listed in Supplemental Table 4. The plasmids *gOML4*, *proACTIN*:*OML4*, *gOML4-GFP*, and *proOML4*:*GUS* were introduced into the *Agrobacterium* strain GV3101. The *gOML4* and *gOML4-GFP* constructs were transferred into *large1-1*, and other plasmids were transferred into the wild type according to a previous report by Hiei et al. (1994).

GUS Staining and Subcellular Localization of OML4

GUS staining of panicles in different developmental stages was performed as previously described by Fang et al. (2016). The GFP fluorescence of *gOML4-GFP* transgenic seedlings was observed using the Zeiss LSM 710 confocal microscope. 4′,6-Diamidino-2-phenylindole (1 μg/mL) was used to stain cell nuclei.

Yeast Two-Hybrid Assays

The cDNA sequences of *GSK2* and *OML4* were amplified using gene-specific primers (Supplemental Table 4), and the products were fused into the linearized *pGADT7* and *pGBKT7* vectors, respectively. Yeast two-hybrid analysis was conducted according to the manufacturer's instructions (Clontech).

BiFC Assay

Full-length cDNA fragments of *OML4* and *GSK2* were recombined into the *pGBW414*-cYFP and *pGBW414-nYFP* vectors. The constructs were

transformed into *Nicotiana benthamiana* mesophyll cells with acetosyringone for transient expression. Confocal imaging analysis was performed using a LSM 710 confocal microscope (Zeiss).

Pull-Down Assay

Recombinant proteins (OML4-MBP and MBP) and prey proteins (GSK2-GST and GST) were incubated in TGH buffer (50 mM Hepes, pH 7.5, 10% glycerol, 150 mM NaCl, Triton X-100, 1.5 mM $MgCl_2$, 1 mM EGTA, and Protease Inhibitor cocktail tablet) for 0.5 h at 4°C with 20 μL of MBP-beads per tube. After centrifugation at 23*g* for 2 min, the supernatant was discarded to stop the reaction. The beads were washed with ice-cold TGH buffer five times, and then 50 μL SDS-loading buffer was added. The samples were denatured at 98°C for 5 min and subjected to the SDS-PAGE analysis. We used anti-MBP (E8032, lot no. 10,009,443; New England Biolabs) and anti-GST (M20007, lot no. 294175; Abmart) to detect the input and the pull-down samples, respectively. Signals were detected using eECL Western Blot Kit (CW0049, Cwbiotech), and images were scanned using Tanon-4500 gel-imaging system according to the manufacturer's instructions.

Coimmunoprecipitation

The *OML4* coding sequence was cloned into the *Kpn*I and *Bam*HI sites of the *pCAMBIA1300-221-Myc* vector to generate the *35S:Myc-OML4* plasmid. The *GSK2* coding sequence was cloned into the *Asc*I and *Pac*I sites of *pMDC43* to generate the *35:GFP-GSK2* plasmid. The constructs were transformed into *N. benthamiana* mesophyll cells with acetosyringone for transient expression. Total protein was isolated with extraction buffer (150 mM NaCl, 50 mM Tris-HCl, 2% Triton X-100, 20% glycerol, 1 mM EDTA, 1× Complete Protease Inhibitor cocktail, and 1 mM phenylmethylsulfonyl fluoride) and incubated with GFP-beads for 40 min at 4°C. After incubation, wash buffer (150 mM NaCl, 50 mM Tris-HCl, 0.1% Triton X-100, 20% glycerol, 1 mM EDTA, and 1× Complete Protease Inhibitor cocktail) was used to wash the beads, and then 50 μL of SDS-loading buffer was added. The samples were denatured at 98°C for 10 min and finally subjected to the SDS-PAGE analysis. We used anti-GFP (M20004, lot no. 313769; Abmart) and anti-MYC (M20002, lot no. 314082; Abmart) to detect the input and immunoprecipitates, respectively. Signals were detected using eECL Western Blot Kit, and images were scanned using a Tanon-4500 gel-imaging system according to the manufacturer's instructions.

Phylogenetic Analysis

To build a phylogenetic tree, Mei2-like proteins were aligned by ClustalX2. The phylogenetic tree was built using this alignment output based on a neighbor-joining method in MEGA7. The parameters used were as follows: complete deletion and bootstrap (1000 replicates).

Phosphorylation Analysis

The coding sequences of *OML4*, *nOML4*, and *cOML4* were amplified using the specific primers (OML4-FLAG-F/R, nOML4-FLAG-F/R, and cOML4-FLAG-F/R) in Supplemental Table 4. The products were cloned to the vector *pETnT* to construct *OML4-FLAG*, *nOML4-FLAG*, and *cOML4-FLAG* plasmids. The *GSK2* coding sequence was amplified using the primers GSK2-GST-F/R and subcloned to the vector *pGEX4T-1* to construct *GSK2-GST* plasmid.

These plasmids were transformed into *Escherichia coli* (host strain BL21). Induction, isolation, and purification of OML4-FLAG, nOML4-FLAG, cOML4-FLAG, and GSK2-GST proteins were done as described previously (Xia et al., 2013). GSK2-GST (10 μL) was incubated with 5 μL of OML4-FLAG, nOML4-FLAG, and cOML4-FLAG in 20 μL of reaction buffer (25 mM Tris-HCl, pH 7.5, 10 mM $MgCl_2$, 1 mM DTT, and 50 mM ATP) for 2 h. Phosphorylated products were analyzed by phos-tag SDS-PAGE. Anti-GST (M20007, lot no. 294175; Abmart) and anti-FLAG (M20008, lot no. 314059; Abmart) antibodies were utilized to detect the phosphorylated products and the input. Signals were detected using eECL Western Blot Kit, and images were scanned using Tanon-4500 gel-imaging system according to the manufacturer's instructions. To detect the phosphorylation sites of OML4, phosphorylated proteins were cut from the SDS-PAGE and digested using trypsin (Sigma-Aldrich) at 37°C overnight. LC-MS/MS was used to analyze the tryptic peptides. Next, these peptides were identified by searching the UniProt database. The Proteome Discoverer software (version 1.3 was used to perform the phosphosite assignment.

BR Treatment

NaClO (30%) was used to sterilize grains. The sterilized grains were grown in 1/2MS medium (Duchefa Biochemie BV) without or with 1 μM epi-BL (Sigma-Aldrich), respectively. After 7 d in a growth incubator (12-h-light/12-h-dark cycle, 3000 lux), the roots were observed for the root waving analysis. For the lamina joint test, the second leaf laminas of 7-d-old seedings were submerged in the solutions containing different epi-BL concentrations.

Domestication Analysis

A sliding window approach was used to analyze the polymorphism levels (π, pairwise nucleotide variation as a measure of variability; Huang et al., 2012). Our analysis was performed for 200-bp windows sliding with 100-bp steps. The 1529 worldwide accessions, including 446 of the wild rice species *Oryza rufipogon* and 1083 of cultivated rice species, were used to analyze the domestication of *OML4* by VCFtools software. To do the genetic analysis, we selected six groups as follows: 446 wild rice species *O. rufipogon*; 155 wild_Or-I (the wild type corresponding to *indica*); 170 wild_Or-III (the wild type corresponding to *japonica*); 484 *japonica* species; 520 *indica* species; and 1083 cultivated rice species.

Accession Numbers

Sequence data from this article can be found in the GenBank/EMBL databases under the following accession numbers: *OML4* (*Os02g0517531*), *GSK2* (*Os05g0207500*).

Supplemental Data

Supplemental Figure 1. Expression level of the indicated genes in ZHJ and *large1-1* panicles.

Supplemental Figure 2. Δ(SNP/INDEL-index) and G' value plots of the whole genome generated from MutMap analysis of *large1-1* mutant alleles.

Supplemental Figure 3. CDS and protein sequence of *OML4*.

Supplemental Figure 4. The plant height, panicle size and grain number per panicle of *gLARGE1;large1-1*.

Supplemental Figure 5. Structural features and phylogenetic tree of OML4.

Supplemental Figure 6. Phylogenetic tree of MEI2-LIKE proteins in plants.

Supplemental Figure 7. *b* and *y* ions peptides map under the mass spectrometric analysis.

Supplemental Figure 8. Alignment of OML4 and its homologs in different plant species.

Supplemental Figure 9. The *large1-1* mutant is more sensitive to brassinolide (BL).

Supplemental Figure 10. Nucleotide diversity analysis of *OML4*.

Supplemental Table 1. Identification of the *large1-1* mutation using the MutMap approach.

Supplemental Table 2. Y2H screening interaction proteins of OML4.

Supplemental Table 3. Phosphopeptides of OML4.

Supplemental Table 4. Primers used in this study.

Supplemental Data Set. Multiple sequence alignment for Supplemental Figures 5B and 6.

ACKNOWLEDGMENTS

We thank Chengcai Chu for the *GSK2-RNAi* vector. This work is supported by grants from the National Natural Science Foundation of China (91735302, 91735304, 31425004, 91535203, 31771340, 31571742, and 31871219), the National Basic Research Program of China (2016YFD0100501, 2016YFD0100400, 2016YFD0100402, 2018 YFD1000700-706-10, and 2017YFD0101701), the National Special Project (2016ZX08009003-003), the Youth Innovation Promotion Association CAS (2019102), and the strategic priority research program of the Chinese Academy of Sciences (XDB27010102).

AUTHOR CONTRIBUTIONS

J.L., D.W., P.D., and Y.H.L. designed experiments. Y.H.L. supervised this project. J.L., D.W., P.D., Y.P.L., D.Z., L.Z., G.D., B.Z., N.L., K.H., Y.J.L., Y.W., and X.H. performed the experiments. J.L., P.D., Y.P.L., Q.Q., and Y.H.L. analyzed data. J.L., P.D., and Y.H.L. prepared figures and wrote the article.

Received June 27, 2019; revised February 28, 2020; accepted April 11, 2020; published April 17, 2020.

REFERENCES

Abe, A., et al. (2012). Genome sequencing reveals agronomically important loci in rice using MutMap. Nat. Biotechnol. **30:** 174–178.

Che, R., Tong, H., Shi, B., Liu, Y., Fang, S., Liu, D., Xiao, Y., Hu, B., Liu, L., Wang, H., Zhao, M., and Chu, C. (2015). Control of grain size and rice yield by GL2-mediated brassinosteroid responses. Nat. Plants **2:** 15195.

Duan, P., Ni, S., Wang, J., Zhang, B., Xu, R., Wang, Y., Chen, H., Zhu, X., and Li, Y. (2015). Regulation of OsGRF4 by OsmiR396 controls grain size and yield in rice. Nat. Plants **2:** 15203.

Duan, P., Rao, Y., Zeng, D., Yang, Y., Xu, R., Zhang, B., Dong, G., Qian, Q., and Li, Y. (2014). SMALL GRAIN 1, which encodes a mitogen-activated protein kinase kinase 4, influences grain size in rice. Plant J. **77:** 547–557.

Duan, P., Xu, J., Zeng, D., Zhang, B., Geng, M., Zhang, G., Huang, K., Huang, L., Xu, R., Ge, S., Qian, Q., and Li, Y. (2017). Natural variation in the promoter of GSE5 contributes to grain size diversity in rice. Mol. Plant **10:** 685–694.

Fan, C., Xing, Y., Mao, H., Lu, T., Han, B., Xu, C., Li, X., and Zhang, Q. (2006). GS3, a major QTL for grain length and weight and minor QTL for grain width and thickness in rice, encodes a putative transmembrane protein. Theor. Appl. Genet. **112:** 1164–1171.

Fang, N., Xu, R., Huang, L., Zhang, B., Duan, P., Li, N., Luo, Y., and Li, Y. (2016). SMALL GRAIN 11 controls grain size, grain number and grain yield in rice. Rice (N. Y.) **9:** 64.

Gao, Y.M., Zhu, J., Song, Y.S., He, C.X., Shi, C.H., and Xing, Y.Z. (2004). Analysis of digenic epistatic effects and QE interaction effects QTL controlling grain weight in rice. J. Zhejiang Univ. Sci. **5:** 371–377.

Guo, T., Chen, K., Dong, N.Q., Shi, C.L., Ye, W.W., Gao, J.P., Shan, J.X., and Lin, H.X. (2018). *GRAIN SIZE AND NUMBER1* negatively regulates the OsMKKK10-OsMKK4-OsMPK6 cascade to coordinate the trade-off between grain number per panicle and grain size in rice. Plant Cell **30:** 871–888.

Heang, D., and Sassa, H. (2012a). Antagonistic actions of HLH/bHLH proteins are involved in grain length and weight in rice. PLoS One **7:** e31325.

Heang, D., and Sassa, H. (2012b). An atypical bHLH protein encoded by POSITIVE REGULATOR OF GRAIN LENGTH 2 is involved in controlling grain length and weight of rice through interaction with a typical bHLH protein APG. Breed. Sci. **62:** 133–141.

Hiei, Y., Ohta, S., Komari, T., and Kumashiro, T. (1994). Efficient transformation of rice (*Oryza sativa* L.) mediated by *Agrobacterium* and sequence analysis of the boundaries of the T-DNA. Plant J. **6:** 271–282.

Hu, J., et al. (2015). A rare allele of GS2 enhances grain size and grain yield in rice. Mol. Plant **8:** 1455–1465.

Hu, Z., et al. (2018). A novel QTL qTGW3 encodes the GSK3/SHAGGY-like kinase OsGSK5/OsSK41 that interacts with OsARF4 to negatively regulate grain size and weight in rice. Mol. Plant **11:** 736–749.

Huang, K., Wang, D., Duan, P., Zhang, B., Xu, R., Li, N., and Li, Y. (2017). WIDE AND THICK GRAIN 1, which encodes an otubain-like protease with deubiquitination activity, influences grain size and shape in rice. Plant J. **91:** 849–860.

Huang, X., et al. (2012). A map of rice genome variation reveals the origin of cultivated rice. Nature **490:** 497–501.

Jeffares, D.C., Phillips, M.J., Moore, S., and Veit, B. (2004). A description of the Mei2-like protein family; structure, phylogenetic distribution and biological context. Dev. Genes Evol. **214:** 149–158.

Kaur, J., Sebastian, J., and Siddiqi, I. (2006). The Arabidopsis-mei2-like genes play a role in meiosis and vegetative growth in Arabidopsis. Plant Cell **18:** 545–559.

Kawakatsu, T., Itoh, J., Miyoshi, K., Kurata, N., Alvarez, N., Veit, B., and Nagato, Y. (2006). PLASTOCHRON2 regulates leaf initiation and maturation in rice. Plant Cell **18:** 612–625.

Lee, C.M., Park, J., Kim, B., Seo, J., Lee, G., Jang, S., and Koh, H.J. (2015). Influence of multi-gene allele combinations on grain size of rice and development of a regression equation model to predict grain parameters. Rice (N. Y.) **8:** 33.

Li, N., and Li, Y. (2016). Signaling pathways of seed size control in plants. Curr. Opin. Plant Biol. **33:** 23–32.

Li, N., Xu, R., and Li, Y. (2019). Molecular networks of seed size control in plants. Annu. Rev. Plant Biol. **70:** 11.1-11.30.

Li, Y., Fan, C., Xing, Y., Jiang, Y., Luo, L., Sun, L., Shao, D., Xu, C., Li, X., Xiao, J., He, Y., and Zhang, Q. (2011). Natural variation in GS5 plays an important role in regulating grain size and yield in rice. Nat. Genet. **43:** 1266–1269.

Liu, J., et al. (2017). GW5 acts in the brassinosteroid signalling pathway to regulate grain width and weight in rice. Nat. Plants **3:** 17043.

Marri, P.R., Sarla, N., Reddy, L.V., and Siddiq, E.A. (2005). Identification and mapping of yield and yield related QTLs from an Indian accession of *Oryza rufipogon*. BMC Genet. **6:** 33.

Si, L., et al. (2016). OsSPL13 controls grain size in cultivated rice. Nat. Genet. **48:** 447–456.

Song, X.J., Huang, W., Shi, M., Zhu, M.Z., and Lin, H.X. (2007). A QTL for rice grain width and weight encodes a previously unknown RING-type E3 ubiquitin ligase. Nat. Genet. **39:** 623–630.

Sun, L., Li, X., Fu, Y., Zhu, Z., Tan, L., Liu, F., Sun, X., Sun, X., and Sun, C. (2013). GS6, a member of the GRAS gene family, negatively regulates grain size in rice. J. Integr. Plant Biol. **55:** 938–949.

Tian, Y., Zheng, H., Zhang, F., Wang, S., Ji, X., Xu, C., He, Y., and Ding, Y. (2019). PRC2 recruitment and H3K27me3 deposition at FLC require FCA binding of COOLAIR. Sci. Adv. **5:** eaau7246.

Tong, H., Liu, L., Jin, Y., Du, L., Yin, Y., Qian, Q., Zhu, L., and Chu, C. (2012). DWARF AND LOW-TILLERING acts as a direct downstream target of a GSK3/SHAGGY-like kinase to mediate brassinosteroid responses in rice. Plant Cell **24:** 2562–2577.

Veit, B., Briggs, S.P., Schmidt, R.J., Yanofsky, M.F., and Hake, S. (1998). Regulation of leaf initiation by the terminal ear 1 gene of maize. Nature **393:** 166–168.

Wan, X.Y., Wan, J.M., Weng, J.F., Jiang, L., Bi, J.C., Wang, C.M., and Zhai, H.Q. (2005). Stability of QTLs for rice grain dimension and endosperm chalkiness characteristics across eight environments. Theor. Appl. Genet. **110:** 1334–1346.

Wang, S., Wu, K., Yuan, Q., Liu, X., Liu, Z., Lin, X., Zeng, R., Zhu, H., Dong, G., Qian, Q., Zhang, G., and Fu, X. (2012). Control of grain size, shape and quality by OsSPL16 in rice. Nat. Genet. **44:** 950–954.

Wang, S., et al. (2015a). The OsSPL16-GW7 regulatory module determines grain shape and simultaneously improves rice yield and grain quality. Nat. Genet. **47:** 949–954.

Wang, Y., et al. (2015b). Copy number variation at the GL7 locus contributes to grain size diversity in rice. Nat. Genet. **47:** 944–948.

Xia, D., Zhou, H., Liu, R., Dan, W., Li, P., Wu, B., Chen, J., Wang, L., Gao, G., Zhang, Q., and He, Y. (2018). GL3.3, a novel QTL encoding a GSK3/SHAGGY-like kinase, epistatically interacts with GS3 to produce extra-long grains in rice. Mol. Plant **11:** 754–756.

Xia, T., Li, N., Dumenil, J., Li, J., Kamenski, A., Bevan, M.W., Gao, F., and Li, Y. (2013). The ubiquitin receptor DA1 interacts with the E3 ubiquitin ligase DA2 to regulate seed and organ size in Arabidopsis. Plant Cell **25:** 3347–3359.

Xiong, G.S., Hu, X.M., Jiao, Y.Q., Yu, Y.C., Chu, C.C., Li, J.Y., Qian, Q., and Wang, Y.H. (2006). Leafy head2, which encodes a putative RNA-binding protein, regulates shoot development of rice. Cell Res. **16:** 267–276.

Xu, R., et al. (2018a). Control of grain size and weight by the OsMKKK10-OsMKK4-OsMAPK6 signaling pathway in rice. Mol. Plant **11:** 860–873.

Xu, R., Yu, H., Wang, J., Duan, P., Zhang, B., Li, J., Li, Y., Xu, J., Lyu, J., Li, N., Chai, T., and Li, Y. (2018b). A mitogen-activated protein kinase phosphatase influences grain size and weight in rice. Plant J. **95:** 937–946.

Ying, J.Z., Ma, M., Bai, C., Huang, X.H., Liu, J.L., Fan, Y.Y., and Song, X.J. (2018). TGW3, a major QTL that negatively modulates grain length and weight in rice. Mol. Plant **11:** 750–753.

Zhai, K., et al. (2019). RRM transcription factors interact with NLRs and regulate broad-spectrum blast resistance in rice. Mol. Cell **74:** 996–1009.e7.

Zhao, D.S., Li, Q.F., Zhang, C.Q., Zhang, C., Yang, Q.Q., Pan, L.X., Ren, X.Y., Lu, J., Gu, M.H., and Liu, Q.Q. (2018). GS9 acts as a transcriptional activator to regulate rice grain shape and appearance quality. Nat. Commun. **9:** 1240.

Zhou, Y., et al. (2015). Natural variations in SLG7 regulate grain shape in rice. Genetics **201:** 1591–1599.